Optimal Routing and Scheduling of Flag State Control Officers in Maritime Transportation

Xizi Qiao [1], Ying Yang [2,*], Yu Guo [2], Yong Jin [2] and Shuaian Wang [2]

1   Tsinghua-Berkeley Shenzhen Institute, Tsinghua University, Shenzhen 518055, China; qxz22@mails.tsinghua.edu.cn
2   Faculty of Business, The Hong Kong Polytechnic University, Hung Hom, Kowloon, Hong Kong 999077, China; christine-yu.guo@connect.polyu.hk (Y.G.); jimmy.jin@polyu.edu.hk (Y.J.); hans.wang@polyu.edu.hk (S.W.)
*   Correspondence: shadow.yang@connect.polyu.hk

Abstract: Maritime transportation plays a pivotal role in the global merchandise trade. To improve maritime safety and protect the environment, every state must effectively control ships flying its flag, which is called flag state control (FSC). However, the existing FSC system is so inefficient that it cannot perform its intended function. In this study, we adopt an optimization method to tackle this problem by constructing an integer programming (IP) model to solve the FSC officer routing and scheduling problem, which aims to maximize the total weight of inspected ships with limited budget and human resources. Then we prove that the IP model can be reformulated into a partially relaxed IP model with the guarantee of the result optimality. Finally, we perform a case study using the Hong Kong port as an example. The results show that our model can be solved to optimality within one second at different scales of the problem, with the ship number ranging from 20 to 1000. Furthermore, our study can be extended by considering the arrangement of working timetables with finer granularity and the fatigue level of personnel.

Keywords: flag state control; ship inspection; routing and scheduling problem; mathematical modeling; maritime transportation

MSC: 90B35

1. Introduction

Maritime transportation plays a pivotal role in facilitating over 80% of global merchandise trade volume. Moreover, the maritime sector constitutes a vital element of national economies, facilitating the import and export of resources. However, it is responsible for nearly 3% of all global greenhouse gas emissions [1]. In order to bolster maritime safety and safeguard the marine environment, the International Maritime Organization (IMO) collaborates with local governments to enforce a series of global and regional conventions [2]. Marine inspection services trace their origins to 1838, following the enactment of congressional legislation aimed at enhancing the safety of steam-propelled vessels [3]. Flag states, whose laws govern the registration or licensing of vessels, play a crucial role in upholding these regulations and international conventions. Flag state control (FSC) guarantees that the ships flying the flag of such state are periodically surveyed by its authorized personnel, called flag state control officers (FSCOs), in order to ensure adherence to relevant standards [4]. A dedicated professional workforce is established and continually refined to ensure that vessels, whether employing antiquated or contemporary technologies, maintain standards of safety for individuals, property, and the environment. Every FSCO undergoes an exhaustive training regimen designed to align with, or surpass, both industry norms and international standards. Hence, these maritime specialists possess comprehensive technical knowledge pertinent to the maritime transportation system, encompassing aspects of vessel components, policies, legislation, and regulations. Currently, marine inspectors

persist in their examination of vessels and the assessment of emergent technologies that aim to mitigate the environmental impact of maritime operations, thereby augmenting both safety and operational efficiency. Therefore, one important response for FSCOs is to inspect substandard ships, which are ships that fall significantly below the required standards for hull, machinery, equipment, or operational safety.

FSC serves the goal of maritime safety and environmental protection. However, certain practical factors lead to the low operational efficiency of FSC, rendering it unable to fulfill its intended purpose effectively. International vessels usually call the ports across various countries, posing challenges for maritime administrations in deploying FSCOs across a broad geographical range. Furthermore, fiscal constraints impose limitations on both the quantity of FSCOs and the extent of their operational scope. Inefficient monitoring practices also pose a constraint. As previously noted, administrations only possess a limited number of human resources for inspection. When the inspection resources of FSC, e.g., the working hours assigned for FSC inspections or the number of available FSCOs, are fixed, inspection efficiency can be improved by optimizing the routing and scheduling plans. Thus, administrations have to arrange the FSCOs carefully so as to maximize the value of manpower within the constraints of limited resources. The corresponding problem can be defined as the FSCO routing and scheduling problem (FSCORSP), which can be classified as the personnel scheduling and routing problem (PSRP). The existing literature studying the PSRP in maritime transportation mainly focuses on the scheduling of personnel, including crews [5–7], pilots [8–10], and so on. However, very few of these works study the scheduling of inspectors [11–13]. Even so, the features and structures of their problems differ from the FSCORSP. This study aims to bridge this gap in this research area with the contributions listed as follows.

First, from a theoretical perspective, we first develop an integer programming (IP) model based on the space–time network modeling approach to solve the FSCORSP in maritime transportation, which simultaneously decides the ships to be inspected by FSCOs and the corresponding travel path of FSCOs. Leveraging the problem characteristics and model structure, we then prove that the IP model can be reformulated into a partially relaxed integer programming (PRIP) model, which is a mixed-integer programming model satisfying an equivalent optimality property.

Second, from a practical perspective, a case study of Hong Kong port is presented to show the performance of both models on instances of various scales. Meanwhile, sensitivity analyses are conducted on multiple parameter settings. The proposed model helps flag state authorities efficiently identify high-risk ships and allocate inspection resources wisely. By targeting substandard ships and reducing unnecessary inspections, it supports flag states in enhancing maritime safety and environmental protection. This approach advances the main goals of the FSC to eliminate substandard shipping and improve overall maritime conditions.

2. Literature Review

The PSRP is the scenario where personnel are mobilized to carry out work-related tasks at diverse locations [14–16]. Accordingly, this problem can be divided into three groups: (1) scheduling, (2) routing, and (3) scheduling and routing [17]. Personnel scheduling aims to build work timetables, including both the content of the tasks and their execution time, for employees within an organization to meet the demand for the services level [18]. Employees must travel between locations to execute the work if each task is situated at a different location. This gives rise to a combination of the personnel scheduling problem and the vehicle routing problem (VRP). The VRP generates one route for each vehicle, aiming at minimizing the total travel distance with the satisfaction of customers' demand [17,19,20]. A route consists of a series of customer locations, with each customer visited only once. The basic version of VRP can be extended in various ways, such as considering multiple trips, multiple depots, and so on, to address complex problems and provide a solid foundation for solving the routing component in the PSRP. Most routing and scheduling problems

can be formulated as network problems. The space–time network offers a compact formulation that accurately represents the movement of commodities over both space and time. This approach has found extensive application in numerous transportation modeling studies [21–24].

Applications for the PSRP can be widely found in different areas. Regarding the scheduling and routing problem for the security personnel, rounds of visits are conducted to various customer premises over a 24 h period in different locations, often using vehicles to travel between locations and then walking within the facilities [24–26]. In the healthcare domain, the home care problem entails local authorities offering community care services to residents. The objective is to efficiently schedule care workers across a region to complete care tasks within specific time windows while minimizing travel time [27–29]. For the airline industry, an important challenge encountered by all airlines is the plan of a daily schedule for a diverse fleet of aircraft. This schedule comprises a series of flight legs that need to be completed by an aircraft, with precise start and finish times specified for each leg at the corresponding airports [30–34]. In the field of maritime transportation, the existing literature mainly applies optimization methods to solve the PSRP, as shown in Table 1. Giachetti et al. [7] introduce mixed-integer linear programming (MILP) models for days-on and days-off scheduling. The first model creates schedules that include two extended, time-limited breaks for each pilot, aiming to minimize workload differences among pilots. The second model allocates the longest possible breaks to employees and seeks to minimize differences in the rest periods accumulated by the pilots. The multi-period inspector scheduling problem (MPISP) first introduced by Qin et al. [13] involves planning routes for a team of inspectors conducting inspections at various locations over several days. The time window of each location within which the inspection can be started is considered. With the aim of maximizing the total completed workload, a tabu search algorithm is designed to generate a lower bound for the MIPSP and an IP model is formulated to generate an upper bound. Compared with the study conducted by Qin et al. [13], Shen et al. [12] endeavor to achieve greater precision by employing an exact algorithm to directly pursue an optimal solution for the MPISP. Rizvanolli and Heise [5] formulate a mixed-integer programming (MIP) model, which ensures that each crew member's work schedule adheres to regulations regarding working and resting hours. The model aims to minimize the number of required crews for a given ship voyage and interruptions during the work. Leggate et al. [6] propose MIP formulations for both the crew scheduling and re-scheduling problems for off-shore supply vessels. The basic model takes the cost of crews as an objective. The re-scheduling problem extends the basic model by considering the recovery-type nature in the real scenario to minimize the cost of possible changes. Xiao et al. [8] study a maritime pilot scheduling problem with working hour regulations. The established MIP model aims to minimize the total operating cost and is solved by a variable neighborhood search algorithm. Jia et al. [9] focus on optimizing seaport operations by addressing the integrated problem of vessel traffic and pilot scheduling. An IP model is developed to minimize costs related to ship tardiness, unmet service needs, and pilot dispatch. The model makes key decisions on the dispatch of pilots and their travel schedules within the port, as well as determining the success of service for each vessel and scheduling the timings for serviced vessels. For the port state control officer (PSCO) assignment and scheduling problem, Yan et al. [11] propose an IP model that determines which ships should be inspected and how to allocate these selected ships to PSCOs, with the goal of maximizing the total number of deficiencies identified during inspections.

Table 1. The PSRP in maritime transportation.

Paper	Problem Features		Model Type	Decisions			Objective
	Scheduling	Routing		ED	WSS	RD	
Giachetti et al. [7]	✓		IP	✓	✓		min amount difference, min dispatch cost
Qin et al. [13]	✓	✓	IP		✓	✓	max completed workload
Rizvanolli and Heise [5]	✓		MIP	✓	✓		min the number of crews and interruptions of tasks
Leggate et al. [6]	✓		MIP		✓		min crew cost, min changes
Shen et al. [12]	✓	✓	IP		✓	✓	max completed workload
Xiao et al. [8]	✓		MIP		✓		min total operating cost
Jia et al. [9]	✓	✓	IP		✓		min total cost of ship tardiness, unmet service needs, and staff dispatch
Lorenzo-Espejo et al. [10]	✓		MILP		✓		min workload difference, min accumulated rest difference
Yan et al. [11]	✓		IP		✓		maximize total weight of inspected ships
Our work	✓	✓	IP, MIP		✓	✓	maximize total weight of inspected ships

Note: IP: integer programming; MIP: mixed-integer programming; MILP: mixed-integer linear programming; ED: employment decision; WSS: working shift schedule; RD: routing decision; max: maximize; min: minimize.

In the aforementioned articles, the MPISP [12,13] and the PSCO assignment and scheduling problem [11] are most relevant to our research problem. However, there are still significant differences between our research question and theirs. In the MPISP, dispatching a team of inspectors to inspect suppliers at various locations resembles the scenario in FSCORSP where FSCOs are dispatched to different ports to inspect ships. Both situations require decisions on routing and scheduling, determining the travel path and the objects to be inspected. However, the difference lies in that, in MPISP, the workload for each supplier is fixed and does not change over time. In contrast, in our problem, we incorporate ship schedule information, including information about the time and location of ships. As the weight and schedule of each ship varies, the set of ships staying at each port dynamically changes over time, where the space–time network is well-suited for modeling. Additionally, since each ship can only be inspected once, it is not possible to directly sum the ship weights at each node to obtain the total weight of nodes in the space–time network. In the PSCO scheduling problem, ship schedule information is considered when making the schedule decision for PSCOs. But this type of problem only involves the work and time scheduling of officers stationed at a single port, without addressing changes in the geographical locations of officers across multiple ports. Consequently, it does not involve decisions regarding routing.

To bridge the gap in the existing literature, we design a tailored modeling approach regarding the problem features of FSC inspection. In Section 3, we extend the detail of problem formulation, including the description of FSCORSP, the space–time network modeling approach, and the mathematical formulation. In the subsequent analysis of the model, we demonstrate the equivalent optimality property. In Section 4, numerical experiments and sensitivity analysis are carried out to verify the model's performance. Finally, Section 5 concludes this work.

3. Problem Formulation

In this section, we first introduce the FSCORSP in Section 3.1. Following that, we provide a comprehensive overview of the modeling framework in relation to the space–time network representation in Section 3.2. Section 3.3 outlines the model formulation of the FSCORSP. Finally, Section 3.4 provides a detailed description of model analysis.

3.1. Description of FSCORSP

The general process of FSC inspection is as follows. A group of FSCOs is dispatched to visit ports in various countries within a specified period to inspect ships flying the flag of its state. It conducts inspection work each day and travels to different ports by airplane during the night. Each ship is assigned a weight to represent the urgency and importance of inspection. The weight can be predicted based on the information of ship characters and

records from prior inspections [11,35,36], which can be treated as a known parameter for the ship in the model. Ships with higher weights are usually high-risk ships. Therefore, in order to ensure the safety of their operation, they have higher priority for inspection. What is more, ships are required to report their schedule of calling each port during the period in advance. Due to the fact that a ship stays for multiple days at each port throughout the entire period and can be inspected at any port, the planning horizon is usually a relatively longer period, e.g., two weeks.

We assume that the Marine Department (MD) collaborates with various ports and maritime authorities and dispatches a team of officers to inspect ships calling at different ports worldwide. A set of ports $\mathcal{P}$ is considered where the officers inspect the ships within a planning horizon with length T. We define one day as a time unit, represented by $t \in \mathcal{T}$, $\mathcal{T} = \{1, \cdots, T\}$. Throughout the planning horizon, each ship $s \in \mathcal{S}$ will call at least one port in $\mathcal{P}$, and the schedule for each ship is already known. If ship s is at the port $p \in \mathcal{P}$ on day $t \in \mathcal{T}$, then the binary parameter δ_{pt}^s is set to 1; otherwise, it is 0. Each ship s is assigned a weight w_s to represent the urgency and importance of inspecting.

We assume that the team dispatched by the MD consists of 2–3 officers who perform tasks together. The team only travels by air at night, which does not interfere with daytime work. That is, the team flies from port $p \in \mathcal{P}$ to port $q \in \mathcal{P}$ in the evening of day $t \in \mathcal{T}$, and inspections can be conducted at port $q \in \mathcal{P}$ during the daytime of day $t + 1$. We define Hong Kong as port 1, where the team initially resides on day 1. They need to be at port 1 by the morning of $T + 1$, meaning if they are not at port 1 on day T, they must fly back to port 1 at least by the evening of day T so that they can arrive at port p the following morning. Accordingly, we denote by $\mathcal{T}_e$ the set containing $\mathcal{T}$ along with the last day $T + 1$, then we have $\mathcal{T}_e = \mathcal{T} \cup \{T + 1\}$. We set the ticket price of the flight from port p to port q as c_{pq} and the overall budget for airplane ticket expenses throughout the entire planning horizon is B. To maintain the efficient turnover of maritime logistics systems, we require that each ship undergo inspection at most once within the planning horizon T, which can occur at any port. Due to the limited inspection resources, a maximum of K ships can be inspected at port $p \in \mathcal{P}$ on day $t \in \mathcal{T}$.

3.2. Space–Time Network Representation

Since the FSCORSP aims to simultaneously determine the routing and scheduling of flag state control officers, we can formulate this problem into the space–time network form.

Figure 1 shows an example of the structure of the space–time network, where port $\mathcal{P} = \{1, 2, 3, 4\}$ is shown as the x–axis and planning horizon with the last day $\mathcal{T}_e = \{1, 2, 3, 4\}$ is shown as the y–axis. Let set $\mathcal{G} = (\mathcal{V}, \mathcal{A})$ denote the space–time network, where $\mathcal{V}$ (indexed by (p, t)) is the set of space–time vertexes and $\mathcal{A}$ (indexed by (p, t, q, r)) is the set of space–time arcs. Using the space–time network, we can visually depict the routing strategy of officers by integrating both their spatial position and the corresponding time. Each vertex (p, t) represents the port $p \in \mathcal{P}$ on day $t \in \mathcal{T}_e$ and each arc (p, t, q, r) denotes the team leaves from port $p \in \mathcal{P}$ in the evening of day $t \in \mathcal{T}$ and arrives at port $q \in \mathcal{P}$ in the morning of day $r \in \mathcal{T}_e$. We assume that any flight requires flying overnight to reach its destination, hence $r = t + 1$. For those arcs (p, t, q, r) with $p = q$, meaning the team is at the same port on both day t and day r, its travel cost $c_{pq} = 0$. Based on the problem setting, we can know that in the underlying space–time network, from each node $(p, t), \forall p \in \mathcal{P}, \forall t \in \mathcal{T}$, there is an edge connecting to node $(p, t + 1)$ and $|\mathcal{P}| - 1$ edges connecting to the nodes in the set $\{(p', t + 1) | \forall p' \in \mathcal{P} \setminus \{p\}\}$.
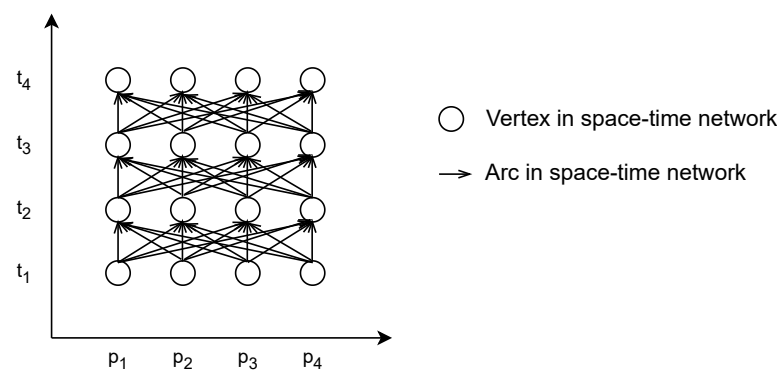
Figure 1. The structure of the space–time network ($|\mathcal{P}| = 4$, $T = 3$).

Based on the underlying network structure, we can find a solution for the routing decision by constructing a path within the graph. A path can be defined as a sequence of vertexes in the space–time network, being expressed as $\mathcal{R} = \{(p, t)|\forall p \in \mathcal{P}, \forall t \in \mathcal{T}_e\}$. It starts from the origin vertex with $(p, t) = (1, 1)$, passes through a series of vertexes with $t \in \mathcal{T} \setminus \{1\}$, and ultimately reaches the destination vertex with $(p, t) = (1, T+1)$. Figure 2 shows an example of the paths for the FSCORSP with $|\mathcal{P}| = 4$, $T = 3$, and $|\mathcal{T}_e| = 4$. The yellow vertex is the origin vertex, representing that the team is located at port 1 on day 1. The red vertex is the destination vertex, which means that the team returns to port 1 on the last day $T + 1$. Path A (dashed line in grey), path B (solid line in red), and path C (dotted line in blue) are the three feasible solutions for the FSCORSP. For path A, officers inspect the ships at port 1 on day 1 and day 2. They leave port 1 in the evening of day 2, fly to port 4, and inspect ships at port 4 on day 3. In the evening of day 3, they take the flight and return to port 1 in the morning of day 4. Accordingly, path A can be expressed as $R_A = \{(1, 1), (1, 2), (4, 3), (1, 4)\}$. Similarly, path B and path C can be represented as $R_B = \{(1, 1), (3, 2), (2, 3), (1, 4)\}$ and $R_C = \{(1, 1), (2, 2), (1, 3), (1, 4)\}$, respectively.
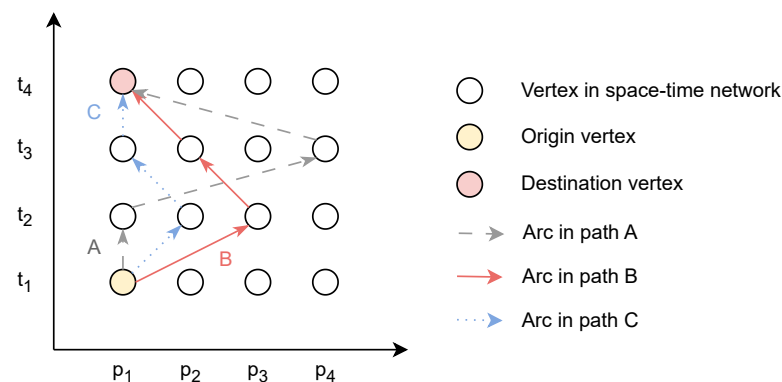
Figure 2. Illustration for FSCORSP in space–time network ($|\mathcal{P}| = 4$, $T = 3$).

3.3. Model Formulation

To enhance the efficiency of the FSC system, we address the FSCORSP through the development of an integer programming (IP) model utilizing the space–time network framework. The primary goal of this model is to optimize the routing and scheduling plans of FSCOs for the ship inspection task, aiming to maximize the total weight of inspected ships while considering constraints such as budget limitations and inspection capacity.

We introduce the binary decision variable x_{pt}, which equals 1 if the team is at port $p \in \mathcal{P}$ on the day $t \in \mathcal{T}_e$, and 0 otherwise. y_{st} is defined as the binary variable, which equals 1 if ship $s \in \mathcal{S}$ is inspected in day $t \in \mathcal{T}$, and 0, otherwise. To describe the flight decision of the team, we use u_{ptqr} as the binary decision variable, which equals 1 if the team flies

from port $p \in \mathcal{P}$ to port $q \in \mathcal{P}$ in the evening of day $t \in \mathcal{T}$, and 0 otherwise. The notation applied in our model is summarized in Table 2.

The model of the FSCORSP can be written as follows:

Table 2. Notations used in the formulation.

Sets	
$\mathcal{T}$	The set of days in the planning horizon T
$\mathcal{T}_e$	The set of days in the planning horizon T and day $T+1$, $\mathcal{T}_e = \mathcal{T} \cup \{T+1\}$
$\mathcal{P}$	The set of ports
$\mathcal{S}$	The set of ships that visit at least one port in $\mathcal{P}$ within planning horizon T
$\mathcal{G}$	The space–time network, $\mathcal{G} = (\mathcal{V}, \mathcal{A})$
$\mathcal{V}$	The set of space–time vertexes, indexed by $(p,t), \forall p \in \mathcal{P}, \forall t \in \mathcal{T}_e$
$\mathcal{A}$	The set of space–time arcs, indexed by $(p,t,q,r), \forall p,q \in \mathcal{P}, \forall t \in \mathcal{T}, r = t+1$
$\mathcal{V}_T$	The set of space–time vertexes, indexed by $(p,t), \forall p \in \mathcal{P}, \forall t \in \mathcal{T}$
Indices	
t, r	The index for days in $\mathcal{T}$ and $\mathcal{T}_e$
p, q	The index for ports in $\mathcal{P}$
s	The index for ships in $\mathcal{S}$
Parameters	
T	The number of days in the planning horizon
w_s	The inspected weight of ship s
δ_{pt}^s	Binary, equals 1 if ship s is at the port p on day t, and 0 otherwise
c_{pq}	The travel cost from port p to port q
B	The overall budget for airplane ticket expenses.
K	The maximum number of ships inspected by the team per day
M	A sufficiently large number
Decision Variables	
x_{pt}	Binary, equals 1 if the team is at space–time vertex (p,t), and 0 otherwise
y_{st}	Binary, equals 1 if ship s is inspected on day t, and 0 otherwise
u_{ptqr}	Binary, equals 1 if the team travels through space–time arc (p,t,q,r), and 0 otherwise

$$\max \quad \sum_{s \in \mathcal{S}} \sum_{t \in \mathcal{T}} w_s y_{st} \tag{1}$$

$$\text{s.t.} \quad x_{1t} = 1, \quad \forall t \in \{1, T+1\}, \tag{2}$$

$$\sum_{p \in \mathcal{P}} x_{pt} = 1, \quad \forall t \in \mathcal{T}_e, \tag{3}$$

$$x_{pt} = \sum_{(q,r) \in \mathcal{V}:(p,t,q,r) \in \mathcal{A}} u_{ptqr}, \quad (p,t) \in \mathcal{V}_T, \tag{4}$$

$$\sum_{(q,r) \in \mathcal{V}:(p,t,q,r) \in \mathcal{A}} u_{ptqr} - \sum_{(q,r) \in \mathcal{V}:(q,r,p,t) \in \mathcal{A}} u_{qrpt} = \begin{cases} 1, & (p,t) = (1,1), \\ -1, & (p,t) = (1, T+1), \\ 0, & \text{otherwise}, \end{cases} \tag{5}$$

$$\sum_{(p,t,q,r) \in \mathcal{A}} u_{ptqr} c_{pq} \leqslant B, \tag{6}$$

$$y_{st} - M \sum_{p \in \mathcal{P}} \delta_{pt}^s x_{pt} \leqslant 0, \quad \forall s \in \mathcal{S}, \forall t \in \mathcal{T}, \tag{7}$$

$$\sum_{t \in \mathcal{T}} y_{st} \leqslant 1, \quad \forall s \in \mathcal{S}, \tag{8}$$

$$\sum_{s \in \mathcal{S}} y_{st} \leqslant K, \quad \forall t \in \mathcal{T}, \tag{9}$$

$$x_{pt} \in \{0,1\}, \quad \forall (p,t) \in \mathcal{V}, \tag{10}$$

$$u_{ptqr} \in \{0,1\}, \quad \forall (p,t,q,r) \in \mathcal{A}, \tag{11}$$

$$y_{st} \in \{0,1\}, \quad \forall s \in \mathcal{S}, \forall t \in \mathcal{T}. \tag{12}$$

The objective function (1) maximizes the total weight of inspected ships. Constraint (2) requires that the team is located at port 1 on day 1 and day $T+1$. Constraint (3) ensures that the team can only be at one port on day $t \in \mathcal{T}_e$. Constraint (4) builds the relationship between the routing plan and the scheduling decision of the team, which indicates that the team is at space–time vertex (p,t) if and only if the team leaves from port $p \in \mathcal{P}$ in the evening of day $t \in \mathcal{T}$. Constraint (5) denotes the flow balance. For the origin vertex $(1,1)$ in the space–time network, the team leaves from port 1 on day 1, therefore its outdegree is 1. For the destination vertex $(1, T+1)$, its indegree is 1. For other vertexes in the space–time network, their outdegree and indegree are equal. Constraint (6) is the budget constraint. Constraint (7) guarantees that if ship $s \in \mathcal{S}$ and the team are not simultaneously at any port on day $t \in \mathcal{T}$, then ship $s \in \mathcal{S}$ can not be inspected on day $t \in \mathcal{T}$. Constraint (8) denotes that ship $s \in \mathcal{S}$ can be inspected at most once throughout the entire planning horizon T. Constraint (9) means that at most K ships can be inspected by the team on the day $t \in \mathcal{T}$. Constraints (10)–(12) are the decision variable constraints.

3.4. Model Analysis

3.4.1. Setting of M

Note that constraint (7) involves the parameter M. According to the existing literature [37], selecting a suitable value for M serves to refine the model and typically enhances its effectiveness during subsequent solution processes. In constraint (7), M should be an upper bound of $y_{st}, \forall s \in \mathcal{S}, \forall t \in \mathcal{T}$. According to constraint (12), y_{st} is the binary decision variable. Therefore, its upper bound is 1, and we can set the corresponding M to 1. Accordingly, the IP model can be written as follows:

$$\max \quad \sum_{s \in \mathcal{S}} \sum_{t \in \mathcal{T}} w_s y_{st} \tag{13}$$

$$\text{s.t.} \quad y_{st} \leqslant \sum_{p \in \mathcal{P}} \delta_{pt}^s x_{pt}, \quad \forall s \in \mathcal{S}, \forall t \in \mathcal{T}, \tag{14}$$

$$\text{Constraints } (2) \sim (6), (8) \sim (12). \tag{15}$$

3.4.2. Equivalent Optimality

In the process of building and analyzing the model, we have an observation: the model where the variables x_{pt} and y_{st} are relaxed to continuous variables, defined as the partially relaxed IP (PRIP) model (Equations (16)–(19)), and the IP model (Equations (13)–(15)) where x_{pt} and y_{st} are binary variables, have the same objective value. Meanwhile, the PRIP model possesses an equivalent optimal integer solution as an optimal solution of the IP model.

$$\max \quad \sum_{s \in \mathcal{S}} \sum_{t \in \mathcal{T}} w_s y_{st} \tag{16}$$

$$\text{s.t.} \quad \text{Constraints } (2) \sim (6), (14), (8), (9), (11), \tag{17}$$

$$0 \leqslant x_{pt} \leqslant 1, \quad \forall (p,t) \in \mathcal{V}, \tag{18}$$

$$0 \leqslant y_{st} \leqslant 1, \quad \forall s \in \mathcal{S}, \forall t \in \mathcal{T}. \tag{19}$$

This phenomenon, referred to as equivalent optimality, inspires us to delve deeper into the structure of the problem and the properties of its optimal solutions. In the subsequent paragraphs of this section, we will provide a theoretical explanation for this observation. We first prove that x_{pt} can be relaxed to continuous variables based on the model structure. After that, the equivalent optimality of y_{st} is demonstrated on the basis of the problem feature.

(1) Equivalent Optimality of x_{pt}

If only the binary variable x_{pt} is relaxed in the IP model (Equations (13)–(15)), then we have the following partially relaxed IP model with relaxed x (PRIP–x model).

$$\max \quad \sum_{s \in \mathcal{S}} \sum_{t \in \mathcal{T}} w_s y_{st} \tag{20}$$

$$\text{s.t.} \quad 0 \leqslant x_{pt} \leqslant 1, \quad \forall (p, t) \in \mathcal{V}, \tag{21}$$

$$\text{Constraints (2)} \sim (6), (8), (9), (11), (12), (14). \tag{22}$$

We can derive the following proposition according to the structure of the PRIP–x model.

Proposition 1. *We can always find an optimal solution (x_l^*, u_l^*, y_l^*) to the PRIP–x model (Equations (20)–(22)) such that it is equivalent to an optimal solution (x^*, u^*, y^*) to the IP model (Equations (13)–(15)).*

Proof. According to constraints (4), we can infer that x_{pt} equals the sum of u_{ptqr}. Since u_{ptqr} is a binary variable, an optimal solution for x_{pt} is also an integer. Therefore, the relaxation of x_{pt} does not affect the optimality of the solution. The PRIP–x model yields an integer optimal solution, equivalent to the solution of the IP model. $\square$

(2) Equivalent Optimality of y_{st}

If only the binary variable y_{st} is relaxed in the IP model (Equations (13)–(15)), then the partially relaxed IP model with relaxed y (PRIP–y model) can be written as

$$\max \quad \sum_{s \in \mathcal{S}} \sum_{t \in \mathcal{T}} w_s y_{st} \tag{23}$$

$$\text{s.t.} \quad 0 \leqslant y_{st} \leqslant 1, \quad \forall s \in \mathcal{S}, \forall t \in \mathcal{T}, \tag{24}$$

$$\text{Constraints (2)} \sim (6), (8) \sim (11), (14). \tag{25}$$

Given any feasible $\bar{x}_{pt}$ and $\bar{u}_{ptqr}$ in the IP model (Equations (13)–(15)), y_{st} can be determined by the IP$(\bar{x}, \bar{u}, y)$ model:

$$\max \quad \sum_{s \in \mathcal{S}} \sum_{t \in \mathcal{T}} w_s y_{st} \tag{26}$$

$$\text{s.t.} \quad y_{st} \leqslant \sum_{p \in \mathcal{P}} \delta_{pt}^s \bar{x}_{pt}, \quad \forall s \in \mathcal{S}, \forall t \in \mathcal{T}, \tag{27}$$

$$\text{Constraints (8), (9), (12).} \tag{28}$$

After relaxing the binary variable y_{st}, we can derive the following LP$(\bar{x}, \bar{u}, y)$ model:

$$\max \quad \sum_{s \in \mathcal{S}} \sum_{t \in \mathcal{T}} w_s y_{st} \tag{29}$$

$$\text{s.t.} \quad \text{Constraints (8), (9), (27).} \tag{30}$$

$$0 \leqslant y_{st} \leqslant 1, \quad \forall s \in \mathcal{S}, \forall t \in \mathcal{T}. \tag{31}$$

Concerning the properties of the optimal solutions for both models, Proposition 2 can be inferred from the characteristics of the problem. For the convenience of problem classification, we define ships with the same weights and schedules as the same group

of ships. In the following context, we prove that Proposition 2 applies to both of these two groups.

Proposition 2. *We can always find an optimal solution y_l^* to the LP$(\bar{x}, \bar{u}, y)$ model (Equations (29)–(31)) such that it is equivalent to an optimal solution y^* to the IP$(\bar{x}, \bar{u}, y)$ model (Equations (26)–(28)).*

Proof. (a) For ships in different groups

We can prove the proposition utilizing proof by contradiction. Consider the case where 4 ships ($\mathcal{S} = \{1, 2, 3, 4\}$) can be inspected on day 1 at the same port. Their weights are $w_1 = 5$, $w_2 = 4$, $w_3 = 3$, and $w_4 = 2$, respectively. The team can inspect at most 2 ships each day ($K = 2$). We assume that an optimal solution is a fractional solution, which is $y_{11} = 0.7$, $y_{21} = 0.6$, $y_{31} = 0.4$, and $y_{41} = 0.3$. Although this solution satisfies the constraints, it is not optimal, because the solution with $y_{11} = 1$ and $y_{21} = 1$ has a better performance, which is an optimal solution in this case. In the maximization problem where ships are all in different groups, an optimal solution selects ships with greater weights with $y = 1$. Therefore, an optimal solution is integer-valued for the case where ships are all in different groups.

(b) For ships in the same group

For ships within the same group, there may exist multiple optimal solutions. For example, if ship 1 and the team stay at the same port from day 1 to day 3, and ship 1 is inspected in an optimal solution, then it is equivalent for the team to inspect ship 1 at any time during the period. Therefore, fractional solutions (e.g., $y_{11} = y_{12} = y_{13} = \frac{1}{3}$) and integer solutions (e.g., $y_{11} = 1$, $y_{12} = y_{13} = 0$) are all optimal solutions. To sum up, when there are multiple optimal solutions for ships within the same group, there always exists an integer optimal solution. $\square$

Based on Proposition 2, the association between the optimal solution properties of the IP model and the PRIP–y model can be revealed in Proposition 3.

Proposition 3. *We can always find an optimal solution (x_l^*, u_l^*, y_l^*) to the PRIP–y model (Equations (23)–(25)) such that it is equivalent to an optimal solution (x^*, u^*, y^*) to the IP model (Equations (13)–(15)).*

Proof. Proposition 2 states that given any feasible $\bar{x}_{pt}$ and $\bar{u}_{ptqr}$ in the IP model, an optimal solution of the IP$(\bar{x}, \bar{u}, y)$ model is equivalent to an optimal solution of the LP$(\bar{x}, \bar{u}, y)$ model. Since an optimal solution (x^*, u^*, y^*) of the IP model also provides a feasible solution, it is equivalent to an optimal solution (x_l^*, u_l^*, y_l^*) obtained by the PRIP–y model. $\square$

Finally, according to Proposition 3 and Proposition 1, we can derive Proposition 4 to give a comprehensive proof to the equivalent optimality observation mentioned at the beginning of this section.

Proposition 4. *We can always find an optimal solution (x_l^*, u_l^*, y_l^*) to the PRIP model (Equations (16)–(19)) such that it is equivalent to an optimal solution (x^*, u^*, y^*) to the IP model (Equations (13)–(15)).*

Proof. Proposition 1 demonstrates that relaxing x_{pt} does not affect the integrality of x_{pt} in an optimal solution of the IP model. The proposition stays true in the PRIP–y model, for it also contains constraints (4) and u_{ptqr} is binary variable. Therefore, x_{pt} can also be relaxed in the PRIP–y model, which is equivalent to the PRIP model. To sum up, after relaxing binary variables, x_{pt} and y_{st}, to be continuous variables, the PRIP model also can derive an integer optimal solution equivalent to the IP model. $\square$

4. Numerical Experiments

In this section, we conduct numerical experiments to analyze the performance of the proposed IP model and evaluate the validity of the equivalent optimality. Meanwhile,

sensitivity analysis is conducted to examine the impact of parameter variations on the results. All experiments are implemented in Python 3.9, using Gurobi 9.5.2 [38] for solving the IP model and the PRIP model. The experiments are conducted on a MacBook Air equipped with an Apple M2 chip, 16 GB of RAM, and the macOS operating system. The parameters of the models are calibrated in preliminary studies and their final values are presented in the following sections.

4.1. Experimental Design

Ship schedules and weights are simulated based on real geographical and flight data, enabling us to make decisions and analyze scenarios that closely mirror real-world situations. We consider six ports ($|\mathcal{P}| = 6$), including Bangkok, Dalian, Hong Kong, Incheon, Shanghai, and Tokyo. A segment refers to a specific leg of a route, typically from an origin port to a destination port. Any two ports in the port set $\mathcal{P}$ can be reached from each other and have multiple segments, and a total of 67 segment records are collected from the website Shipxy (Shipxy: https://routes.shipxy.com/, accessed on 10 April 2024). Since the flight time of the team can only occur during non-working hours to avoid disrupting daytime inspection work, we query the flight ticket prices from the website Google Flights (Google Flights: https://www.google.com/travel/flights, accessed on 11 April 2024) for each segment from the origin port to the destination port on 28 April 2024. Additionally, the flight time period is selected for non-working hours.

As shown in Table 3, we include the average information of the segments between any two ports, where "ID" represents the index of each segment. "Distance" is the average sailing distance in nautical miles (nm) between two ports, "Travel time" represents the average travel time of the segment in days (d), "Speed" denotes the average speed in knots (kn) of the ship traveling on this segment, and "Price" is the price of the flight ticket in US dollars (USD) from the origin port to the destination port. For the six ports, there are 67 segments in total, which are then used to generate the schedule for each ship.

We choose a two-week planning horizon, i.e., $T = 14$, with a one-day time unit and set the total ship number $|\mathcal{S}| = 60$. The weight of the ships follows a uniform distribution within the range of $[0, 1]$. A route of ship s is defined as a series of consecutive segments traveling through the entire planning horizon T. We define $\mathcal{P}_s$ as the port set containing the ports on the route of ship $s \in \mathcal{S}$. At the beginning of the planning horizon when $t = 1$, all the ships are at the origin port of their first segment p_1^s. The duration time of ship s staying at port $p \in \mathcal{P}_s$, d_s, is randomly sampled from a closed interval $[D_{\min}, D_{\max}]$ of integers with equal probability, where $D_{\min}$ is the minimum duration time and $D_{\max}$ is the maximum duration time. We assume that each ship departs from the origin port only in the morning. The earliest inspection can be conducted on the day after the ship arrives at the destination port.

The routes for all the ships are generated based on all the segments, and then the route information is converted into the schedule information within the planning horizon. The schedule information for part of the ships, which serves as the parameter δ_{pt}^s in the IP model, is listed in Table 4. Each item in the "Ship schedule" represents the duration of the ship staying at the port. The ports are represented by the initial letters of their names, where "B" stands for Bangkok, "D" is Dalian, "H" is Hong Kong, "I" is Incheon, "S" is Shanghai, and "T" is Tokyo. The time range is represented by a closed interval to indicate the range of days during which the ship stays at the port. Taking ship 1 as an example, it stays at Tokyo on day 1 and day 2. Then it travels from Tokyo to Dalian from day 3 and day 6. Then it is at Dalian on day 7 and day 8. After that, ship 1 goes back to Tokyo from day 9 to day 13 and is located at Tokyo on day 14.

Table 3. The average information for the segments and their flight ticket prices.

ID	Origin Port	Destination Port	Distance (nm)	Travel Time (d)	Speed (kn)	Price (USD)
1	Bangkok	Dalian	2850.90	7.92	15.00	554
2	Bangkok	Hong Kong	1551.00	5.88	11.00	153
3	Bangkok	Incheon	2772.80	10.70	10.80	343
4	Bangkok	Shanghai	2306.50	10.52	10.80	288
5	Bangkok	Tokyo	3143.50	11.39	11.50	344
6	Dalian	Bangkok	2720.90	11.93	9.50	166
7	Dalian	Hong Kong	1314.03	4.65	12.40	183
8	Dalian	Incheon	275.70	0.85	15.23	162
9	Dalian	Shanghai	551.53	2.38	9.93	264
10	Dalian	Tokyo	1250.37	3.83	13.73	711
11	Hong Kong	Bangkok	1363.95	5.06	11.90	155
12	Hong Kong	Dalian	1306.63	4.26	13.27	395
13	Hong Kong	Incheon	1213.15	3.10	16.40	229
14	Hong Kong	Shanghai	851.33	3.36	10.67	208
15	Hong Kong	Tokyo	1628.30	4.63	15.85	136
16	Incheon	Bangkok	2530.90	9.96	10.60	147
17	Incheon	Dalian	274.23	1.17	10.70	146
18	Incheon	Hong Kong	1223.25	3.52	14.55	221
19	Incheon	Shanghai	496.37	2.79	7.60	115
20	Incheon	Tokyo	1069.20	4.42	10.20	207
21	Shanghai	Bangkok	2282.63	9.14	10.60	221
22	Shanghai	Dalian	549.80	2.33	9.85	159
23	Shanghai	Hong Kong	851.23	6.01	8.53	168
24	Shanghai	Incheon	490.90	2.61	8.87	170
25	Shanghai	Tokyo	1037.57	3.07	14.53	530
26	Tokyo	Bangkok	3143.50	11.19	11.70	333
27	Tokyo	Dalian	1168.30	3.48	14.15	367
28	Tokyo	Hong Kong	1629.00	4.21	16.40	150
29	Tokyo	Incheon	1026.07	10.10	5.37	129
30	Tokyo	Shanghai	1036.20	3.40	12.80	582

Table 4. The schedule information for part of the ships.

| Ship ID	Ship Schedule	Ship ID	Ship Schedule
1	[(T, [1, 2]), (D, [7, 8]), (T, [14, 14])]	11	[(I, [1, 3]), (S, [8, 10])]
2	[(D, [1, 1]), (I, [4, 4]), (S, [9, 9])]	12	[(B, [1, 1]), (D, [10, 10])]
3	[(B, [1, 1]), (D, [10, 10])]	13	[(B, [1, 1]), (H, [8, 8]), (I, [13, 13])]
4	[(D, [1, 1]), (H, [8, 8]), (B, [13, 13])]	14	[(I, [1, 3]), (H, [8, 10])]
5	[(D, [1, 1]), (T, [6, 6]), (S, [11, 11])]	15	[(I, [1, 3]), (H, [8, 10])]
6	[(I, [1, 3]), (S, [7, 9]), (T, [14, 14])]	16	[(I, [1, 3]), (B, [14, 14])]
7	[(I, [1, 3]), (S, [7, 9]), (D, [13, 14])]	17	[(S, [1, 2]), (B, [14, 14])]
8	[(S, [1, 2]), (D, [6, 7]), (H, [14, 14])]	18	[(H, [1, 3]), (D, [9, 11]), (I, [13, 14])]
9	[(D, [1, 1]), (H, [8, 8]), (D, [14, 14])]	19	[(H, [1, 3]), (S, [8, 10])]
10	[(T, [1, 2]), (S, [7, 8]), (D, [12, 13])]	20	[(D, [1, 1]), (H, [8, 8]), (D, [14, 14])]

The parameters of the experiments are set as shown in Table 5. Generally, we conduct 151 experiments with experiment ID (EID) ranging from 0 to 150. Each of the experiments is included in the corresponding group with a group ID (GID). $G0$, $G1$, and $G2$ are the groups of experiments that aim to illustrate the performance of the IP model in solving instances with different ship numbers ($|\mathcal{S}|$). Accordingly, the results of $G3$, $G4$, and $G5$ are generated by the PRIP model. As for the sensitivity analysis, experiments in $G6$ are set with divergence budgets. $G7$ is designed for testing the performance of experiments with variable duration time intervals (DTI), and $G8$ is set with different inspection capacities (IC). "MT" represents the model type, including the IP model (IP) and the PRIP model (PRIP). In the "$|\mathcal{S}|$", "Budget (USD)", and "IC" columns, $[a, b, c]$ represents a list of numbers generated from a to b with a step size of c. The closed intervals in the "DTI" column have the same meaning as the duration time interval $[D_{\min}, D_{\max}]$ mentioned above.

Table 5. Experiment parameter settings.

GID	EID	$|\mathcal{S}|$	Budget (USD)	DTI	IC	MT
G0	0–9	[20,200,20]	5000	[1,3]	3	IP
G1	10–29	[220,600,20]	5000	[1,3]	3	IP
G2	30–49	[620,1000,20]	5000	[1,3]	3	IP
G3	50–59	[20,200,20]	5000	[1,3]	3	PRIP
G4	60–79	[220,600,20]	5000	[1,3]	3	PRIP
G5	80–99	[620,1000,20]	5000	[1,3]	3	PRIP
G6	100–119	300	[0,3800,200]	[1,3]	3	PRIP
G7	120–140	300	4000	[1,1],[1,2],[1,3],[1,4], [1,5],[1,6],[2,2],[2,3], [2,4],[2,5],[2,6],[3,3], [3,4],[3,5],[3,6],[4,4], [4,5],[4,6],[5,5],[5,6], [6,6]	3	PRIP
G8	141–150	300	4000	[1,3]	[1,10,1]	PRIP

4.2. Performance of the IP Model and the PRIP Model

In this section, we analyze the performance of the IP model as well as the PRIP model. Figures 3 and 4 show the optimal results of the IP model and the PRIP model, respectively. The *x*–axis represents the experiment ID, where instances are arranged in increasing order of the number of ships. The *y*–axis corresponds to the values of indicators, including the number of ships ($|\mathcal{S}|$), the objective of an optimal solution (Obj), the inspected ship number (ISN), the total flight cost (TFC), and the total number of flights (TNF).

(**a**) Obj of instances.

(**b**) ISN of instances.

(**c**) TFC of instances.

(**d**) TNF of instances.
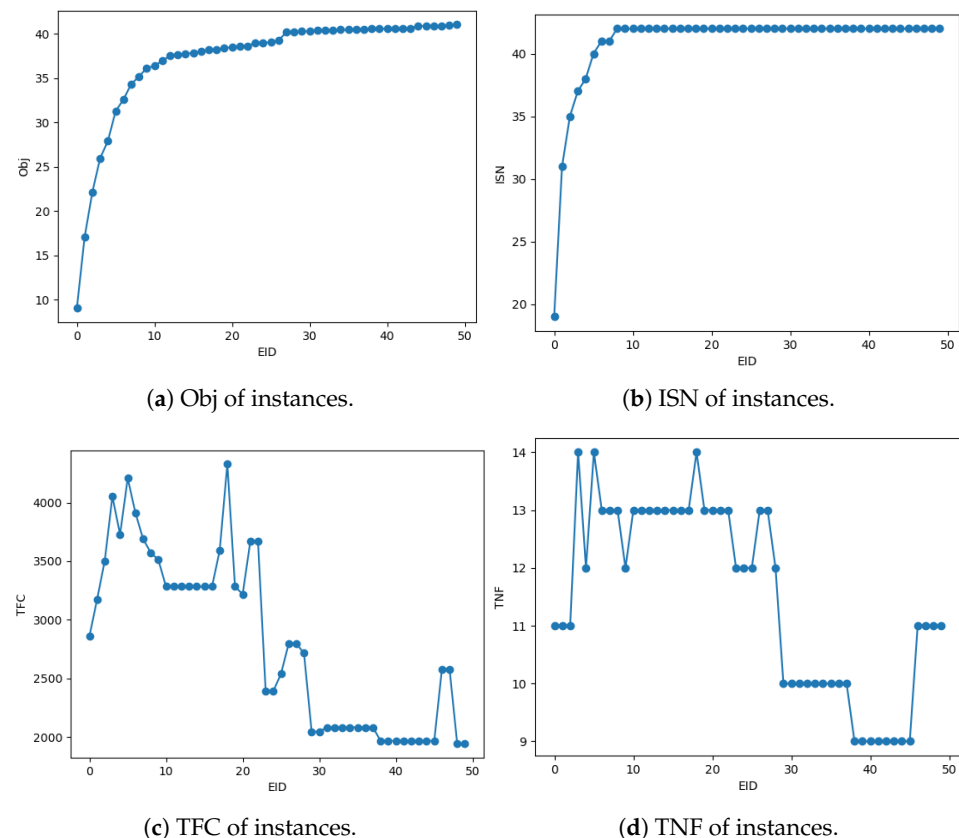
Figure 3. Optimal results of the IP model for small-scale instances (EID: 0–49).

(**a**) Obj of instances.

(**b**) ISN of instances.

(**c**) TFC of instances.
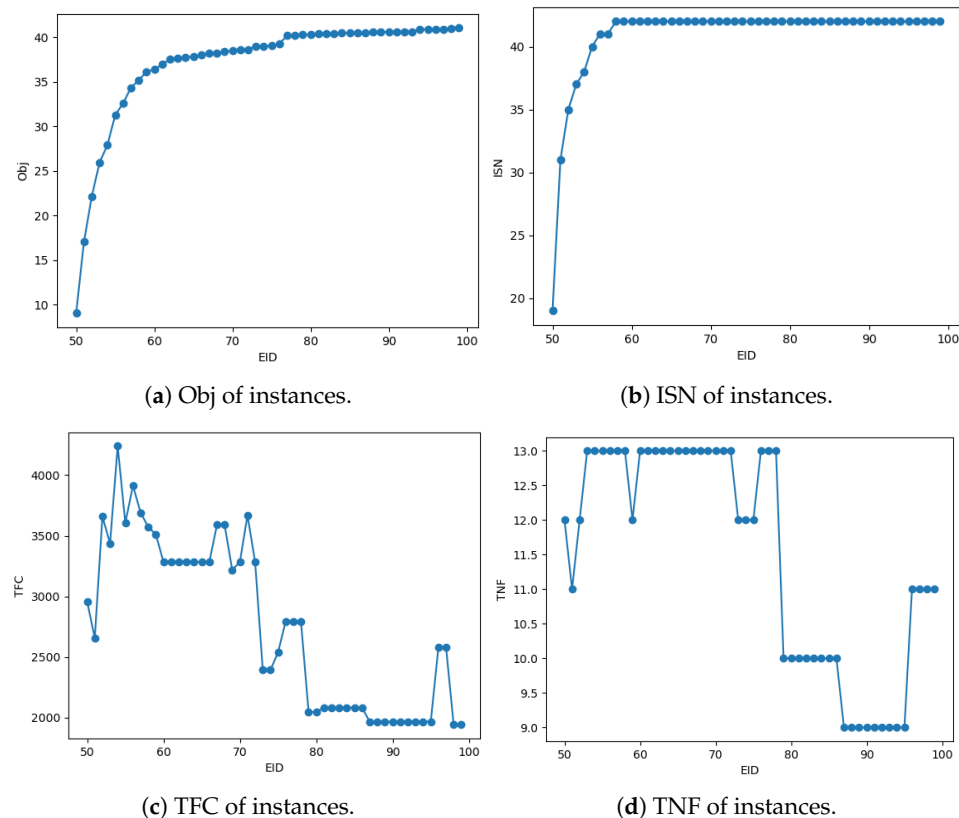

(**d**) TNF of instances.

Figure 4. Optimal results of the PRIP model for small-scale instances (EID: 50–99).

As shown in Figures 3 and 4, the IP model and the PRIP model generally yield identical results for the Obj and ISN indicators across similar instances. However, differences arise in the TFC and TNF values for certain instances generated by the two models, although many remain the same. As for the performance of each indicator, both Obj and ISN demonstrate an increasing trend as the set size $|\mathcal{S}|$ grows. Specifically, for Obj, as depicted in Figures 3a and 4a, there is a noticeable rapid growth in the early stages for groups $G0$ and $G3$. This growth becomes more moderate during the mid-term phases ($G1$ and $G4$), and eventually, the increase in Obj tapers off, showing a gradual convergence in the later stages ($G2$ and $G5$). In contrast, the ISN value surges to 42 with increasing $|\mathcal{S}|$ and remains constant beyond this point, as shown in Figures 3b and 4b. The TFC and TNF values start high but significantly decrease in the mid-stage. The following analysis will further dissect these trends for a more nuanced understanding. Additionally, it is noteworthy that Obj, which measures the overall objective value, reflects the effectiveness of the models in optimizing against set constraints and targets, underlining its pivotal role in assessing model performance.

To comprehensively illustrate the results, we divide all instances into three categories based on the number of ships: small-scale, medium-scale, and large-scale. Tables 6 and 7 present the optimal solution results obtained by the IP model and the PRIP model, respectively, for small-scale instances, with the number of ships ranging from 20 to 200. From the results in Table 6, we can observe that as the number of ships increases, both the Obj and the ISN show a significant increase. The Obj of the instance with $|\mathcal{S}| = 20$ is 9.02, while the Obj of the instance with $|\mathcal{S}| = 200$ increases to 36.12. This is mainly due to the fact that as the total number of ships increases, the actual number of ships inspected gradually increases, as long as the number of inspected ships does not reach the inspection capacity limit of the team. Since the objective function is the sum of the weights of the inspected ships, the objective function increases accordingly. CPU time refers to the solution time consumed by solving the model. As the "CPU time" column shows in Table 6, the average

solution time consumed by solving the IP model is 0.09 seconds. Therefore, it is quite efficient to solve small-scale cases by directly using Gurobi as the solver.

Table 6. Optimal results of the IP model for small-scale instances (EID: 0–49).

EID	$|\mathcal{S}|$	Obj	ISN	TFC (USD)	TNF	CPU Time (s)
	20	9.02	19	2858	11	0.02
	40	17.04	31	3173	11	0.05
	60	22.13	35	3502	11	0.08
	80	25.95	37	4053	14	0.07
	100	27.89	38	3728	12	0.09
0–9	120	31.26	40	4208	14	0.12
	140	32.56	41	3914	13	0.23
	160	34.31	41	3691	13	0.07
	180	35.16	42	3573	13	0.09
	200	36.12	42	3511	12	0.10
Avg	110	27.14	36.60	3621.10	12.40	0.09

Table 7. Optimal results of the PRIP model for small-scale instances (EID: 50–59).

EID	$|\mathcal{S}|$	Obj	ISN	TFC (USD)	TNF	CPU Time (s)
	20	9.02	19	2958	12	0.02
	40	17.04	31	2656	11	0.04
	60	22.13	35	3659	12	0.09
	80	25.95	37	3437	13	0.08
	100	27.89	38	4240	13	0.08
50–59	120	31.26	40	3606	13	0.11
	140	32.56	41	3914	13	0.23
	160	34.31	41	3691	13	0.08
	180	35.16	42	3573	13	0.10
	200	36.12	42	3511	12	0.10
Avg	110	27.14	36.60	3524.50	12.50	0.09

For the same instances, Table 7 presents the results obtained by the PRIP model. We can observe that the Obj and ISN values obtained by the PRIP model are identical to those obtained by the IP model. The average values of TFC obtained by the two models are relatively close, with USD 3621.10 for the IP model and USD 3524.50 for the PRIP model. However, TFC and TNF are not entirely identical, indicating that the flight paths are not entirely the same. This is because there are multiple optimal solutions for the same instance. Therefore, it is possible to have the same Obj but different TFC values for the same instance. The time taken to solve small-scale cases using the PRIP model is roughly the same as that taken by the IP model, with an average of 0.09 seconds for both.

For the results of medium-scale instances generated by the IP model, we observe from the results in Table 8 that as the number of ships increases, the ISN becomes a constant value of 42, while the Obj gradually increases. The ISN remains constant because of the existence of the total inspection capacity limit. In the experiments, the total planning horizon T is 14 and the inspection capacity of each day K equals 3. Therefore, the team can only inspect at most 42 ships during the planning horizon. When the number of ships is large enough to reach the total inspection capacity, there is no means to increase Obj by increasing ISN, but Obj can be improved by choosing the ships with larger weights. The expansion of the solution space due to the increase in total ship number allows the team to select ships with larger weights for inspection without changing the overall number of inspected ships. Therefore, the Obj is able to increase slightly.

Table 8. Optimal results of the IP model for medium-scale instances (EID: 10–29).

EID	$|\mathcal{S}|$	Obj	ISN	TFC (USD)	TNF	CPU Time (s)
	220	36.37	42	3283	13	0.09
	240	36.94	42	3283	13	0.14
	260	37.52	42	3283	13	0.09
	280	37.66	42	3283	13	0.13
	300	37.72	42	3283	13	0.14
	320	37.85	42	3283	13	0.17
	340	38.01	42	3283	13	0.15
	360	38.20	42	3590	13	0.12
	380	38.21	42	4328	14	0.20
	400	38.42	42	3283	13	0.18
10–29	420	38.45	42	3219	13	0.23
	440	38.62	42	3669	13	0.22
	460	38.62	42	3669	13	0.24
	480	38.97	42	2392	12	0.24
	500	38.97	42	2392	12	0.22
	520	39.04	42	2538	12	0.25
	540	39.26	42	2795	13	0.20
	560	40.16	42	2795	13	0.24
	580	40.19	42	2716	12	0.27
	600	40.26	42	2046	10	0.25
Avg	410	38.47	42.00	3120.65	12.70	0.19

The results obtained by the PRIP model for instances of medium scale still yield the same Obj as the IP model as shown in Table 9, with TFC values not entirely identical but having similar average values. The average TFC value is USD 3068.40, which decreases by 14.86% compared to the average TFC of USD 3524.50 for small-scale instances. For medium-scale cases, the average solution times for the IP model and the PRIP model are similar, with 0.19 seconds and 0.20 seconds, respectively, which is double the average solution time for small-scale cases.

Table 9. Optimal results of the PRIP model for medium-scale instances (EID: 60–79).

EID	$|\mathcal{S}|$	Obj	ISN	TFC (USD)	TNF	CPU Time (s)
	220	36.37	42	3283	13	0.11
	240	36.94	42	3283	13	0.15
	260	37.52	42	3283	13	0.10
	280	37.66	42	3283	13	0.17
	300	37.72	42	3283	13	0.13
	320	37.85	42	3283	13	0.14
	340	38.01	42	3283	13	0.15
	360	38.20	42	3590	13	0.16
	380	38.21	42	3590	13	0.21
	400	38.42	42	3219	13	0.24
60–79	420	38.45	42	3283	13	0.21
	440	38.62	42	3669	13	0.23
	460	38.62	42	3283	13	0.29
	480	38.97	42	2392	12	0.20
	500	38.97	42	2392	12	0.22
	520	39.04	42	2538	12	0.21
	540	39.26	42	2795	13	0.21
	560	40.16	42	2795	13	0.23
	580	40.19	42	2795	13	0.28
	600	40.26	42	2046	10	0.28
Avg	410	38.47	42.00	3068.40	12.70	0.20

Compared with medium-scale instances, where the magnitude of increase in $|\mathcal{S}|$ is the same, the optimal solutions of large-scale instances also reach the inspection capacity limit but exhibit only a slight rise in Obj from 40.26 to 41.02 as shown in Tables 10 and 11. This is because although $|\mathcal{S}|$ continues to increase, the distribution of weights for newly added ships remains the same as those that already exist. Therefore, when ISN reaches its limit, even as the overall number of candidate ships increases, its contribution to the Obj is small.

Hence, the Obj does not exhibit significant growth. The average CPU times consumed by solving the IP model and the PRIP model are 0.39 seconds and 0.36 seconds, indicating that the models can also quickly obtain optimal solutions for large-scale cases.

Table 10. Optimal results of the IP model for large-scale instances (EID: 30–49).

EID	$|\mathcal{S}|$	Obj	ISN	TFC (USD)	TNF	CPU Time (s)
	620	40.26	42	2046	10	0.27
	640	40.38	42	2082	10	0.24
	660	40.38	42	2082	10	0.28
	680	40.38	42	2082	10	0.29
	700	40.44	42	2082	10	0.31
	720	40.44	42	2082	10	0.32
	740	40.44	42	2082	10	0.33
	760	40.44	42	2082	10	0.34
	780	40.57	42	1967	9	0.37
	800	40.57	42	1967	9	0.38
30–49	820	40.57	42	1967	9	0.39
	840	40.57	42	1967	9	0.39
	860	40.57	42	1967	9	0.40
	880	40.61	42	1967	9	0.42
	900	40.87	42	1967	9	0.40
	920	40.87	42	1967	9	0.41
	940	40.88	42	2579	11	0.51
	960	40.90	42	2579	11	0.52
	980	41.00	42	1941	11	0.57
	1000	41.02	42	1941	11	0.58
Avg	810	40.61	42.00	2069.80	9.80	0.39

Table 11. Optimal results of the PRIP model for large-scale instances (EID: 80–99).

EID	$|\mathcal{S}|$	Obj	ISN	TFC (USD)	TNF	CPU Time (s)
	620	40.26	42	2046	10	0.28
	640	40.38	42	2082	10	0.30
	660	40.38	42	2082	10	0.31
	680	40.38	42	2082	10	0.32
	700	40.44	42	2082	10	0.32
	720	40.44	42	2082	10	0.33
	740	40.44	42	2082	10	0.33
	760	40.44	42	1967	9	0.33
	780	40.57	42	1967	9	0.34
	800	40.57	42	1967	9	0.33
80–99	820	40.57	42	1967	9	0.36
	840	40.57	42	1967	9	0.35
	860	40.57	42	1967	9	0.36
	880	40.61	42	1967	9	0.37
	900	40.87	42	1967	9	0.38
	920	40.87	42	1967	9	0.38
	940	40.88	42	2579	11	0.51
	960	40.90	42	2579	11	0.41
	980	41.00	42	1941	11	0.49
	1000	41.02	42	1941	11	0.48
Avg	810	40.61	42.00	2064.05	9.75	0.36

The average TFC of large-scale instances generated by the PRIP model, which is USD 2064.0, has a decrease of 42.84% compared to the one obtained by using the same model to solve small-scale instances. Accordingly, the average TNF decreases from 12.4 to 9.75. This phenomenon is caused by the increase in $|\mathcal{S}|$ for the following reasons. Assuming the team completes the inspection of K ships with relatively large weights at port p on day t, if there are still K ships with higher weights awaiting inspection at port p on day $t + 1$ (including ships that stay at port p on days t and $t + 1$, as well as ships that arrive at port p on day t and can be inspected on day $t + 1$), then the team will still stay at port p on day $t + 1$ without the need for consecutive nightly flights. Consequently, the overall TNF will decrease.

This scenario is more likely to occur when $|\mathcal{S}|$ is high. If there are fewer ships, then after completing the inspection on day t, there may be no ships to inspect on day $t + 1$ at the same port. Even if there are ships available for inspection, the sum of weights of the uninspected ships at port p on day $t + 1$ may be relatively small, and thus may not be included in an optimal solution. In such cases, the team needs to fly to another port with larger sums of weights for uninspected ships.

4.3. Sensitivity Analysis

In this section, we analyze how the variation of parameters would influence the performance of the PRIP model. To be concise, three groups of sensitivity analysis are performed: (1) divergence of the budget; (2) variation of the duration time; (3) difference of the inspection capacity.

4.3.1. Divergence of the Budget

Figure 5 gives an overall review of the optimal results of the PRIP model for instances in $G6$ with different budgets. We can see that all four indicators gradually increase with the increase in budget. Table 12 provides us with additional details, from which we can know that if the budget is even smaller than the price of flights leaving from the original port, then the team will stay at port 1 during the planning horizon and only can inspect ships at port 1. Experiments with EID $= 100$ and EID $= 101$ correspond to this scenario. Therefore, given the same setting of ships, they share the same value of the four indicators. When the team has enough budget to leave port 1, Obj increases accordingly with the increase in budget and converges to 37.72 until the budget exceeds TFC.
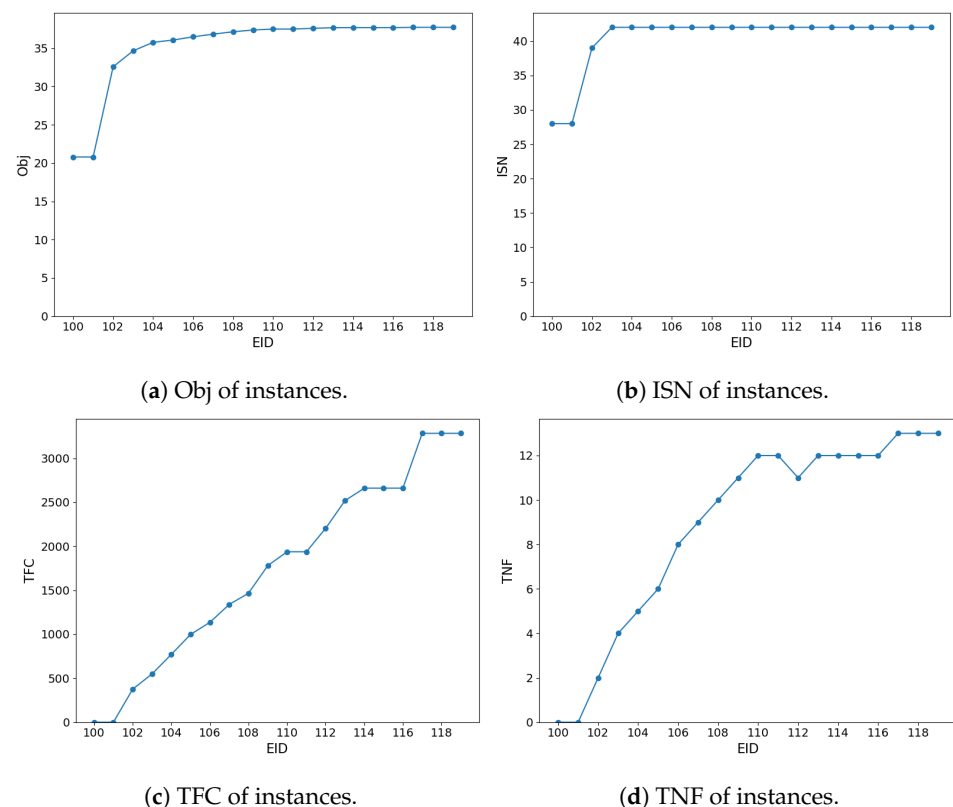

(**a**) Obj of instances.

(**b**) ISN of instances.

(**c**) TFC of instances.

(**d**) TNF of instances.

Figure 5. Optimal results of instances with different budgets (EID: 100–119).

Table 12. Optimal results of instances with different budgets (EID: 100–119).

EID	Budget (USD)	Obj	ISN	TFC (USD)	TNF	CPU Time (s)
	0	20.79	28	0	0	0.07
	200	20.79	28	0	0	0.07
	400	32.57	39	376	2	0.16
	600	34.65	42	548	4	0.22
	800	35.76	42	771	5	0.48
	1000	36.06	42	998	6	0.70
	1200	36.48	42	1135	8	0.68
	1400	36.83	42	1338	9	0.76
	1600	37.14	42	1466	10	0.62
	1800	37.37	42	1780	11	0.52
100–119	2000	37.49	42	1937	12	0.29
	2200	37.49	42	1937	12	0.48
	2400	37.59	42	2204	11	0.28
	2600	37.67	42	2518	12	0.21
	2800	37.68	42	2660	12	0.20
	3000	37.68	42	2660	12	0.19
	3200	37.68	42	2660	12	0.19
	3400	37.72	42	3283	13	0.16
	3600	37.72	42	3283	13	0.16
	3800	37.72	42	3283	13	0.16
Avg	1900	35.24	40.45	1741.85	8.85	0.33

4.3.2. Variation of the Duration Time

Figure 6 shows that when changing the duration time of ship $s \in \mathcal{S}$ staying at port $p \in \mathcal{P}$, which is defined as d_s, the values of the four indicators fluctuate around their respective means. Combining the data from Table 13, it can be observed that for experiments with EID of 120, 126, 131, 135, 138 and 140, ISN is 39, while ISN for the other experiments is equal to 42. Further observation of the duration time parameters for these instances reveals that $D_{\min} = D_{\max}$, which indicates that the duration time for all ships is identical within each instance.
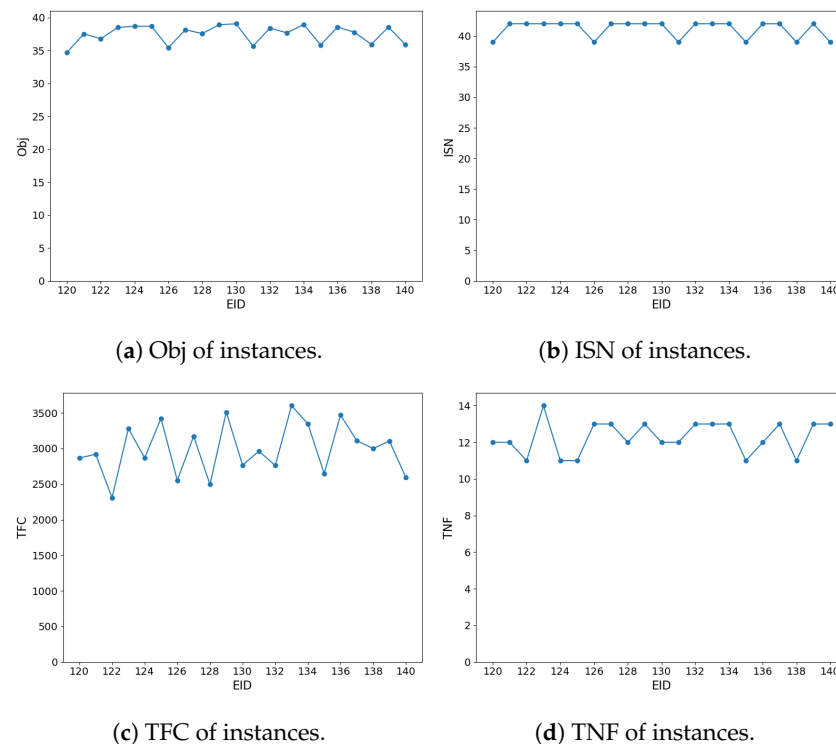

(**a**) Obj of instances.

(**b**) ISN of instances.

(**c**) TFC of instances.

(**d**) TNF of instances.

Figure 6. Optimal results of instances with different duration time (EID: 120–140).

Table 13. Optimal results of instances with different duration time (EID: 120–140).

EID	DTI	Obj	ISN	TFC (USD)	TNF	CPU Time (s)
	[1,1]	34.74	39	2868	12	0.08
	[1,2]	37.55	42	2918	12	0.12
	[1,3]	36.79	42	2307	11	0.16
	[1,4]	38.52	42	3281	14	0.17
	[1,5]	38.70	42	2867	11	0.30
	[1,6]	38.68	42	3423	11	0.39
	[2,2]	35.46	39	2552	13	0.24
	[2,3]	38.17	42	3172	13	0.27
	[2,4]	37.59	42	2495	12	0.30
	[2,5]	38.93	42	3511	13	0.42
120–140	[2,6]	39.08	42	2765	12	0.22
	[3,3]	35.68	39	2962	12	0.48
	[3,4]	38.42	42	2761	13	0.29
	[3,5]	37.71	42	3601	13	0.36
	[3,6]	38.97	42	3347	13	0.23
	[4,4]	35.87	39	2647	11	0.32
	[4,5]	38.58	42	3470	12	0.20
	[4,6]	37.79	42	3109	13	0.22
	[5,5]	35.95	39	3000	11	0.21
	[5,6]	38.58	42	3104	13	0.23
	[6,6]	35.95	39	2596	13	0.23
Avg	-	37.51	41.14	2988.38	12.29	0.26

Hence, we can deduce the reason for such results under this scenario. From Table 3, we can ascertain that the minimum travel time for a segment is 0.85 days. Additionally, since ships can only be inspected starting from the day after they arrive at a port, if all ships depart from port 1 on day t after staying for the same duration time, then no ships can be inspected on day t. Furthermore, due to the number of ships being large enough ($|\mathcal{S}| = 300$), as indicated by Table 8, the optimal ISN in the solution can reach the upper limit of the total inspection limit, which is 42. Therefore, by delaying inspections for one day, i.e., inspecting K fewer ships, a total of 39 ships can ultimately be inspected in an optimal solution.

4.3.3. Difference of the Inspection Capacity

From Figure 7 and Table 14, it can be observed that as IC increases, both Obj and ISN continue to grow, while TFC and TNF fluctuate within a certain range. Assuming an infinite supply of candidate ships, ISN would then be the sum of reaching the inspection capacity limit each day. We define the ISN in this ideal scenario as ISN*, i.e., ISN* = IC $\times T$. If $|\mathcal{S}|$ is smaller compared to ISN*, then ISN* = ISN. However, if $|\mathcal{S}|$ is not sufficiently large, it may lead to a situation where the number of ships inspected at the port each day in an optimal solution is less than K, then we have ISN* > ISN.

Table 14. Optimal results of instances with different inspection capacities (EID: 141–150).

EID	IC	Obj	ISN	TFC (USD)	TNF	CPU Time (s)
	1	13.55	14	2508	14	0.12
	2	26.37	28	2853	12	0.13
	3	37.72	42	3283	13	0.20
	4	48.33	56	3283	13	0.13
	5	57.83	70	3305	13	0.16
141–150	6	66.80	84	3783	13	0.25
	7	74.75	98	3783	13	0.21
	8	82.14	112	2757	12	0.26
	9	88.96	125	2757	12	0.30
	10	95.29	138	3560	14	0.20
Avg	5.50	59.17	76.70	3187.20	12.90	0.19

(**a**) Obj of instances.

(**b**) ISN of instances.

(**c**) TFC of instances.
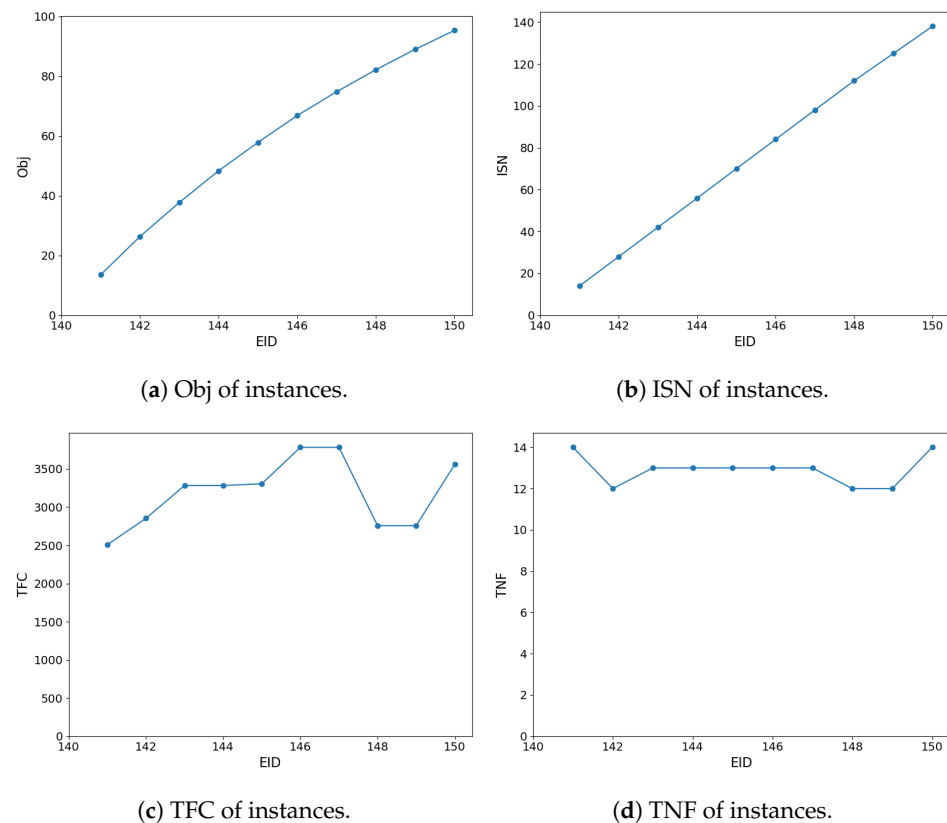

(**d**) TNF of instances.

Figure 7. Optimal results of instances with different inspection capacities (EID: 141–150).

To sum up, the results of the numerical experiments show that the IP model and the PRIP model share the same Obj and ISN for the same instance. It is worth mentioning that for some cases, there are multiple optimal solutions, which is reflected in the differences between TFC and TNF results in the IP and PRIP models for these cases. For the average results obtained solving the IP model, for small-scale cases, an average of 110 ships are candidates for inspection, with the optimal solution involving an average inspection of 36.6 ships, and an Obj of 27.14. For medium-scale cases, the average value of the ship number is 410, with the optimal solution involving an average inspection of 42 ships, and an Obj of 38.47. For large-scale cases, the average value of the ship number is 810, with the optimal solution again involving an average inspection of 42 ships, and an Obj of 40.61. Regarding the efficiency of solving all the instances, the CPU time of solving two models to optimality by Gurobi ranges from 0.02 seconds to 0.76 seconds, with an average value of 0.26 seconds. From the results of the sensitivity analysis, it is evident that when changing the budget amount, the duration time of ships, and the inspection capacity, our model shows a stable performance. The model constructed in this paper is a simplified abstraction of the FSCORSP, considering only basic decisions such as personnel routing planning and ship inspection selection. Future work could consider more realistic problem settings, such as incorporating decisions regarding staff work timetables and measuring employee fatigue levels.

5. Conclusions

In order to protect the marine environment and guarantee maritime safety, flag states must implement necessary measures by periodically inspecting their ships by qualified FSCOs. However, realistic factors such as a larger scope of activities, limited financial resources, and inefficient operational modes contribute to the low efficiency of FSC.

Motivated by the above facts, we construct an IP model and solve it to optimality for the FSCORSP, which simultaneously considers the ship schedule information and the FSCO routing and scheduling with the aim of maximizing the total weight of inspected

ships. Based on the model structure, we prove that after relaxing part of the binary decision variables to continuous variables, the PRIP model can generate the same optimal objective value as the one obtained by the IP model when solving the same instance. Furthermore, we can always find an optimal solution to the PRIP model such that it is equivalent to an optimal solution to the IP model. In the numerical experiments, we use the Hong Kong port as an example to conduct the case study. The results show that the two models share the same optimal objective. For the large-scale instance, the instance with 1000 ships waiting to be inspected can be solved to optimality in 0.58 seconds, with 42 ships being inspected and the optimal Obj equals 41.02. All the instances can be solved in 0.26 seconds on average.

This study marks the first attempt to formulate a mathematical optimization model that incorporates ship schedule information to enhance FSC efficiency. While the models demonstrate strong potential in improving inspection scheduling, they also reveal critical dynamics in operational efficiency influenced by the scale of shipping operations. The investigation highlights the need for future enhancements in modeling aspects such as work-life balance and inspection capacity optimization, laying a foundation for further research into the FSCORSP. Further exploration can determine the optimal balance between total ship numbers and daily inspection capacities, aiming to minimize uninspected ships while maximizing daily inspection capabilities. Additionally, the development of heuristic and exact algorithms to address the complexities of FSCORSP represents a promising direction for future research.

Author Contributions: Conceptualization, S.W.; methodology, X.Q., Y.Y., Y.G., Y.J. and S.W.; software, X.Q.; validation, X.Q.; formal analysis, X.Q.; investigation, X.Q., Y.Y. and S.W.; resources, S.W. and Y.G.; data curation, X.Q. and Y.Y.; writing—original draft preparation, X.Q., Y.Y., Y.G., Y.J. and S.W.; writing—review and editing, X.Q. and Y.Y. and S.W.; visualization, X.Q.; supervision, S.W.; project administration, S.W.; funding acquisition, Y.G. All authors have read and agreed to the published version of the manuscript.

Data Availability Statement: Data are contained within the article.

Conflicts of Interest: The authors declare no conflicts of interest.

References

1. UNCTAD. Review of Maritime Transport 2023. 2023. Available online: https://unctad.org/publication/review-maritime-transport-2023 (accessed on 11 April 2024).
2. Yan, R.; Wang, S.; Zhen, L.; Laporte, G. Emerging approaches applied to maritime transport research: Past and future. *Commun. Transp. Res.* **2021**, *1*, 100011. [CrossRef]
3. USCG. Flag State Control 2022 Domestic Annual Report. 2023. Available online: https://www.dco.uscg.mil/Our-Organization/Assistant-Commandant-for-Prevention-Policy-CG-5P/Inspections-Compliance-CG-5PC-/Commercial-Vessel-Compliance/Domestic-Compliance-Division/CVC1AnnualReport/ (accessed on 10 April 2024).
4. Alderton, T.; Winchester, N. Flag states and safety: 1997–1999. *Marit. Policy Manag.* **2002**, *29*, 151–162. [CrossRef]
5. Rizvanolli, A.; Heise, C.G. Efficient ship crew scheduling complying with resting hours regulations. In Proceedings of the Operations Research Proceedings 2016: Selected Papers of the Annual International Conference of the German Operations Research Society (GOR), Helmut Schmidt University Hamburg, Hamburg, Germany, 30 August–2 September 2016; Springer: Berlin/Heidelberg, Germany, 2018; pp. 535–541.
6. Leggate, A.; Sucu, S.; Akartunalı, K.; van der Meer, R. Modelling crew scheduling in offshore supply vessels. *J. Oper. Res. Soc.* **2018**, *69*, 959–970. [CrossRef]
7. Giachetti, R.E.; Damodaran, P.; Mestry, S.; Prada, C. Optimization-based decision support system for crew scheduling in the cruise industry. *Comput. Ind. Eng.* **2013**, *64*, 500–510. [CrossRef]
8. Xiao, L.; Wang, Z.; Tan, Z.; Wang, C. A solution method for the maritime pilot scheduling problem with working hour regulations. *Asia-Pac. J. Oper. Res.* **2021**, *38*, 2040015. [CrossRef]
9. Jia, S.; Wu, L.; Meng, Q. Joint scheduling of vessel traffic and pilots in seaport waters. *Transp. Sci.* **2020**, *54*, 1495–1515. [CrossRef]
10. Lorenzo-Espejo, A.; Muñuzuri, J.; Onieva, L.; Cortés, P. Scheduling consecutive days off: A case study of maritime pilots. *Comput. Ind. Eng.* **2021**, *155*, 107192. [CrossRef]
11. Yan, R.; Wang, S.; Cao, J.; Sun, D. Shipping domain knowledge informed prediction and optimization in port state control. *Transp. Res. Part B Methodol.* **2021**, *149*, 52–78. [CrossRef]

12. Shen, H.; Shu, S.; Qin, H.; Wu, Q. An exact algorithm for the multi-period inspector scheduling problem. *Comput. Ind. Eng.* **2020**, *145*, 106515. [CrossRef]

13. Qin, H.; Ming, W.; Zhang, Z.; Xie, Y.; Lim, A. A tabu search algorithm for the multi-period inspector scheduling problem. *Comput. Oper. Res.* **2015**, *59*, 78–93. [CrossRef]

14. Castillo-Salazar, J.A.; Landa-Silva, D.; Qu, R. Workforce scheduling and routing problems: Literature survey and computational study. *Ann. Oper. Res.* **2016**, *239*, 39–67. [CrossRef]

15. Dahite, L.; Kadrani, A.; Benmansour, R.; Guibadj, R.N.; Fonlupt, C. Multi-objective model and variable neighborhood search algorithms for the joint maintenance scheduling and workforce routing problem. *Mathematics* **2022**, *10*, 1807. [CrossRef]

16. Zuo, Z.; Li, Y.; Fu, J.; Wu, J. Human resource scheduling model and algorithm with time windows and multi-skill constraints. *Mathematics* **2019**, *7*, 598. [CrossRef]

17. Raff, S. Routing and scheduling of vehicles and crews: The state of the art. *Comput. Oper. Res.* **1983**, *10*, 63–211. [CrossRef]

18. Ernst, A.T.; Jiang, H.; Krishnamoorthy, M.; Sier, D. Staff scheduling and rostering: A review of applications, methods and models. *Eur. J. Oper. Res.* **2004**, *153*, 3–27. [CrossRef]

19. Desrochers, M.; Desrosiers, J.; Solomon, M. A new optimization algorithm for the vehicle routing problem with time windows. *Oper. Res.* **1992**, *40*, 342–354. [CrossRef]

20. Braekers, K.; Ramaekers, K.; Van Nieuwenhuyse, I. The vehicle routing problem: State of the art classification and review. *Comput. Ind. Eng.* **2016**, *99*, 300–313. [CrossRef]

21. Tong, L.; Zhou, X.; Miller, H.J. Transportation network design for maximizing space-time accessibility. *Transp. Res. Part B Methodol.* **2015**, *81*, 555–576. [CrossRef]

22. Li, P.; Mirchandani, P.; Zhou, X. Solving simultaneous route guidance and traffic signal optimization problem using space-phase-time hypernetwork. *Transp. Res. Part B Methodol.* **2015**, *81*, 103–130. [CrossRef]

23. Zhang, L.; Meng, Q.; Fwa, T.F. Big AIS data based spatial-temporal analyses of ship traffic in Singapore port waters. *Transp. Res. Part E Logist. Transp. Rev.* **2019**, *129*, 287–304. [CrossRef]

24. Guan, Y.; Xiang, W.; Wang, Y.; Yan, X.; Zhao, Y. Bi-level optimization for customized bus routing serving passengers with multiple-trips based on state-space-time network. *Phys. A Stat. Mech. Its Appl.* **2023**, *614*, 128517. [CrossRef]

25. Lau, H.C.; Yuan, Z.; Gunawan, A. Patrol scheduling in urban rail network. *Ann. Oper. Res.* **2016**, *239*, 317–342. [CrossRef]

26. Surendonk, T.J.; Chircop, P.A. On the computational complexity of the patrol boat scheduling problem with complete coverage. *Nav. Res. Logist.* **2020**, *67*, 289–299. [CrossRef]

27. Di Mascolo, M.; Martinez, C.; Espinouse, M.L. Routing and scheduling in home health care: A literature survey and bibliometric analysis. *Comput. Ind. Eng.* **2021**, *158*, 107255. [CrossRef]

28. Naderi, B.; Begen, M.A.; Zaric, G.S.; Roshanaei, V. A novel and efficient exact technique for integrated staffing, assignment, routing, and scheduling of home care services under uncertainty. *Omega* **2023**, *116*, 102805. [CrossRef]

29. Bazirha, M.; Kadrani, A.; Benmansour, R. Stochastic home health care routing and scheduling problem with multiple synchronized services. *Ann. Oper. Res.* **2023**, *320*, 573–601. [CrossRef]

30. Wen, X.; Sun, X.; Sun, Y.; Yue, X. Airline crew scheduling: Models and algorithms. *Transp. Res. Part Logist. Transp. Rev.* **2021**, *149*, 102304. [CrossRef]

31. Wen, X.; Ma, H.L.; Chung, S.H.; Khan, W.A. Robust airline crew scheduling with flight flying time variability. *Transp. Res. Part E Logist. Transp. Rev.* **2020**, *144*, 102132. [CrossRef]

32. Wen, X.; Chung, S.H.; Ma, H.L.; Khan, W.A. Airline crew scheduling with sustainability enhancement by data analytics under circular economy. In *Annals of Operations Research*; Springer: Berlin/Heidelberg, Germany, 2023; pp. 1–27.

33. Graf, V.; Teichmann, D.; Dorda, M.; Kontrikova, L. Dynamic model of contingency flight crew planning extending to crew formation. *Mathematics* **2021**, *9*, 2138. [CrossRef]

34. Ahmed, M.B.; Hryhoryeva, M.; Hvattum, L.M.; Haouari, M. A matheuristic for the robust integrated airline fleet assignment, aircraft routing, and crew pairing problem. *Comput. Oper. Res.* **2022**, *137*, 105551. [CrossRef]

35. Yang, Z.; Yang, Z.; Yin, J. Realising advanced risk-based port state control inspection using data-driven Bayesian networks. *Transp. Res. Part A Policy Pract.* **2018**, *110*, 38–56. [CrossRef]

36. Wu, S.; Chen, X.; Shi, C.; Fu, J.; Yan, Y.; Wang, S. Ship detention prediction via feature selection scheme and support vector machine (SVM). *Marit. Policy Manag.* **2022**, *49*, 140–153. [CrossRef]

37. Lübbecke, M.E. Column generation. *Wiley Encycl. Oper. Res. Manag. Sci.* **2010**, *17*, 18–19.

38. *Gurobi Optimizer Reference Manual*; Gurobi Optimization, LLC: Beaverton, OR, USA, 2022.